Electronic Supplementary Materials

Ultrafine Fe-modulated Ni nanoparticles embedded within nitrogen-doped carbon from Zr-MOFs-confined conversion for efficient oxygen evolution reaction

Lingtao Kong, Zhouxun Li, Hui Zhang, Mengmeng Zhang, Jiaxing Zhu, Mingli Deng **(✉)**, Zhenxia Chen, Yun Ling, Yaming Zhou

Shanghai Key Laboratory of Molecular Catalysis and Innovative Materials, Department of Chemistry, Fudan University, Shanghai 200433, China

E-mail: mldeng@fudan.edu.cn

1. Material and methods

All reagents were purchased from commercial sources and used as received without further purification.

Synthesis of UiO-67. 4,4'-biphenyl dicarboxylic acid (H_2bpdc, 121.1 mg, 0.50 mmol), $ZrCl_4$ (116.5 mg, 0.50 mmol) and benzoic acid (1.832 g, 15.00 mmol) were placed in a scintillation bottle with 40 mL dimethylformamide (DMF). After stirring for 30 min at room temperature, the mixture was transferred into a 80 mL Teflon-lined stainless-steel container and heated at 120 °C for 24 h. After cooling down to room temperature, the polycrystalline samples were obtained by centrifugation and rinsed with DMF for three times. Then, the solids were soaked in acetone for 3 d, and the solution was exchanged with fresh acetone every 12 h. After 3 d of soaking, the solids were collected via centrifugation and dried under vacuum.

Synthesis of Ni_1Fe_1UiO-67. The procedure for preparation of Fe_1Ni_1UiO-67 was similar to that of UiO-67 except adding $Ni(NO_3)_2 \cdot 6H_2O$ (73 mg, 0.25 mmol) / $Fe(NO_3)_3 \cdot 9H_2O$ (101 mg, 0.25 mmol) to the above solution. Note that the subscript of Ni_1Fe_1UiO-67 stands for the feeding mole ratio of Ni and Fe, for the sake of simplicity.

The as-made UiO-67 was placed in a quartz boat. Under the flow of N_2 (99.99 %) with a rate of 50 mL min^{-1}, the temperature was increased with a rate of 2 °C min^{-1} from room temperature to 600°C, and kept for 2 h. After cooling down to room temperature under the flow of N_2, black powder was obtained. It is marked as UiO-67-600.

Ni_1Fe_1UiO-67 was carbonized with the same pyrolysis process of UiO-67-600, and the resultant samples were marked as Ni_1Fe_1UiO-67-600.

2. Characterization

Powder X-ray diffraction (PXRD) patterns were measured using a Bruker D8 powder diffractometer at 40 kV, 40 mA for Cu *K*α radiation (λ = 1.5406 Å), with a scan speed of 0.2 s/step and a step size of 0.05°. The phase purity of the bulk products was determined by comparison of the simulated and experimental PXRD patterns.

Thermogravimetric analysis (TGA) experiments were carried out on a Mettler Tolepo TGA/SDTA 851 analyzer in the temperature range 30~800 °C under nitrogen flow with a heating rate of 10 °C·min^{-1}. High-Resolution Transmission Electron Microscopy (HRTEM) measurements were conducted on a JEM-2100 microscope (JEOL, Japan) operated at 200 kV.

Scanning electron microscope mapping (SEM-mapping) measurement was tested on FEI Nova Nano-Sem 450 scanning electron microscope with voltage of 15kV. X-ray photoelectron spectroscopy (XPS) was recorded on a Perkin Elmer PHI 5000C ESCA system (Perkin Elmer, USA). Inductively coupled plasma atomic emission spectroscopy (ICP-AES) were measured using a PerkinElmer Avio 200 Optical Emission Spectrometer. Fourier transform infrared spectroscopy (FT-IR) was applied to identify the local vibration environment of these samples. Before measurement, all samples were dried. A Varian 670 FTIR spectrophotometer was used to perform sample analysis. Thirty-two scans were collected at a resolution of 4 cm^{-1}.

Brunauer-Emmett-Teller (BET) surface area and BJH pore distribution measurements were collected at 77 K by N_2 on a micromeritics ASAP 2020 adsorption analyzer. The as-made sample (about 100 mg) was evacuated on a vacuum line overnight at room temperature. The sample was then transferred to a pre-weighed sample tube and degassed at 200 °C for 24h. The sample tube was re-weighed to obtain a consistent mass for the degassed exchanged MOF.

3. Electrochemical tests

All electrochemical measurements, including linear sweep voltammetry (LSV), cyclic voltammetry (CV) and electrochemical impedance spectroscopy (EIS) were performed in a typical three-electrode setup using an electrochemical workstation (CHI 760D, ChenHua Instruments Co. Ltd., Shanghai, China) in nitrogen-purged KOH (1.0 mol·L^{-1}) at room temperature. A glassy carbon electrode (GCE, 3 mm in diameter, ChenHua Instruments Co. Ltd., Shanghai, China) loaded with a catalyst, carbon electrode, and a Hg/HgO were used as working electrode, counter electrode, and reference electrode, respectively. For the working electrode, 2 mg of catalyst inks

were dispersed in 1ml of water by sonication to obtain a homogeneous ink. Then, 5 μL of ink was loaded onto a GCE and dried in oven under 50 °C with 5 min. Then 5 μL of Nafion solution (5 wt %) (Alfa Aesar) was dropwise added to GCE with the following drying in oven under 50 °C.

Cyclic voltammograms (CVs) were measured from 0.854 to 0.954 V versus RHE in 1 M KOH (A.R) solution at a scan range of 20 ~ 120 mV s^{-1}. Then, the linear sweep voltammetry (LSV) with a scan rate of 5 mV s^{-1} was recorded in the same solution, and all the LSV values were iR-corrected. The potentials were converted to a reversible hydrogen electrode (RHE). The durability of catalysts was evaluated by taking continuous 4000 CV cycles at a scan rate of 100 mV s^{-1}. After 4000 cycles, the LSV measurement was again performed under the same conditions. The potentials were converted to those vs a reversible hydrogen electrode (RHE), as following equation: $E_{RHE}=E_{SCE} + 0.059\times pH+0.098$ V.

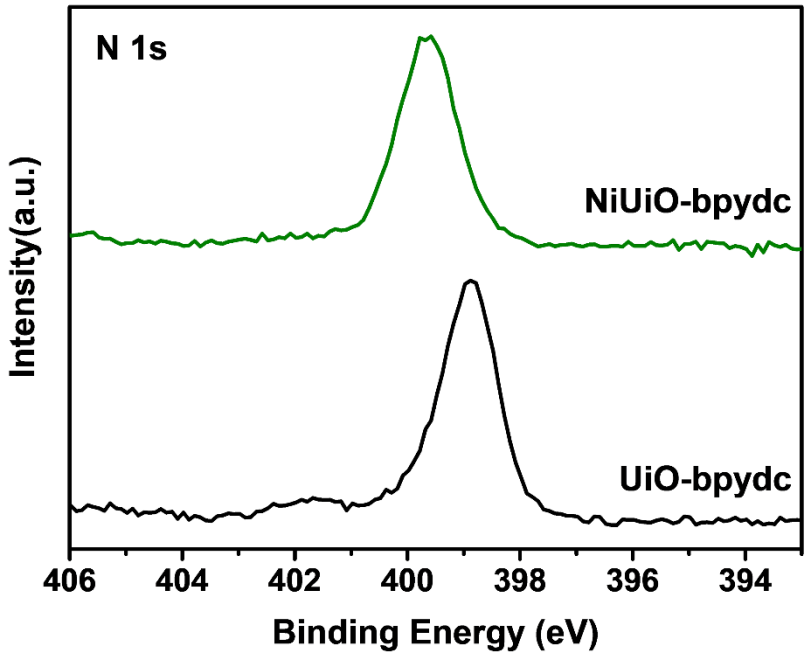

Figure S1. High-resolution N 1s XPS spectra of UiO-bpydc and NiUiO-bpydc.

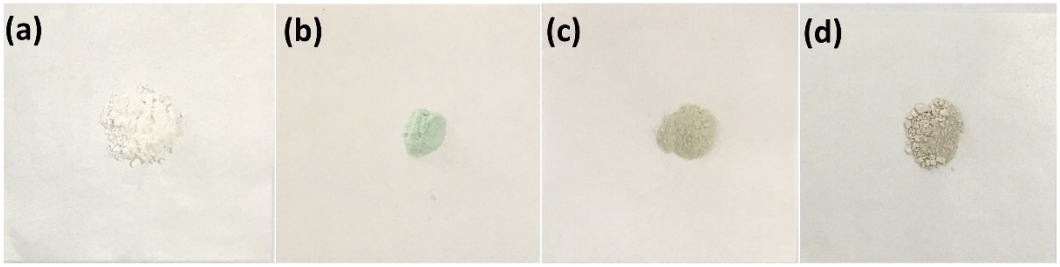

Figure S2. The optical photographs of UiO-bpydc(a), NiUiO-bpydc (b), Ni_1Fe_1UiO-bpydc(c), FeUiO-bpydc(d).

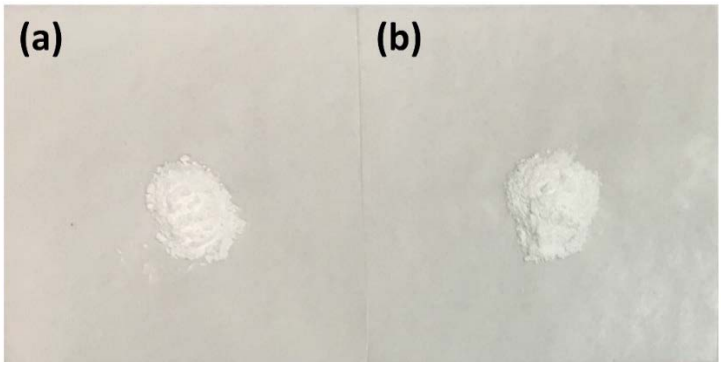

Figure S3. The optical photographs of UiO-67 (a), Ni_1Fe_1UiO-67 (b).

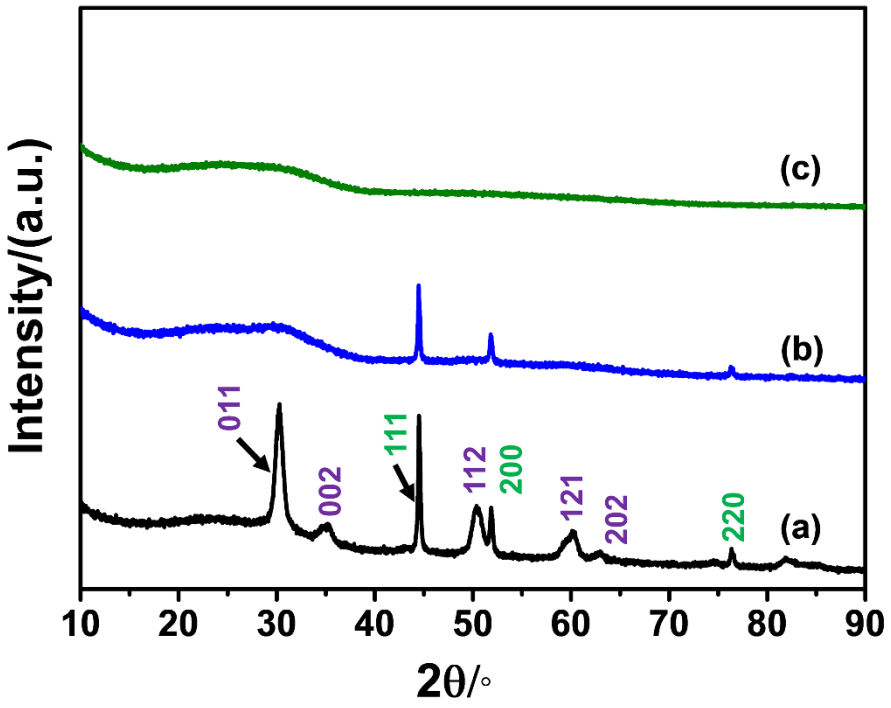

Figure S4. PXRD patterns of these NiUiO-bpydc-600 (a), Ni_1Fe_1UiO-bpydc-600 (b) and FeUiO-bpydc-600 (c) by the pyrolysis of the corresponding samples under 600 °C (Green: PDF# 87-0712, Metallic Ni; Purple: PDF#50-1089, ZrO_2).

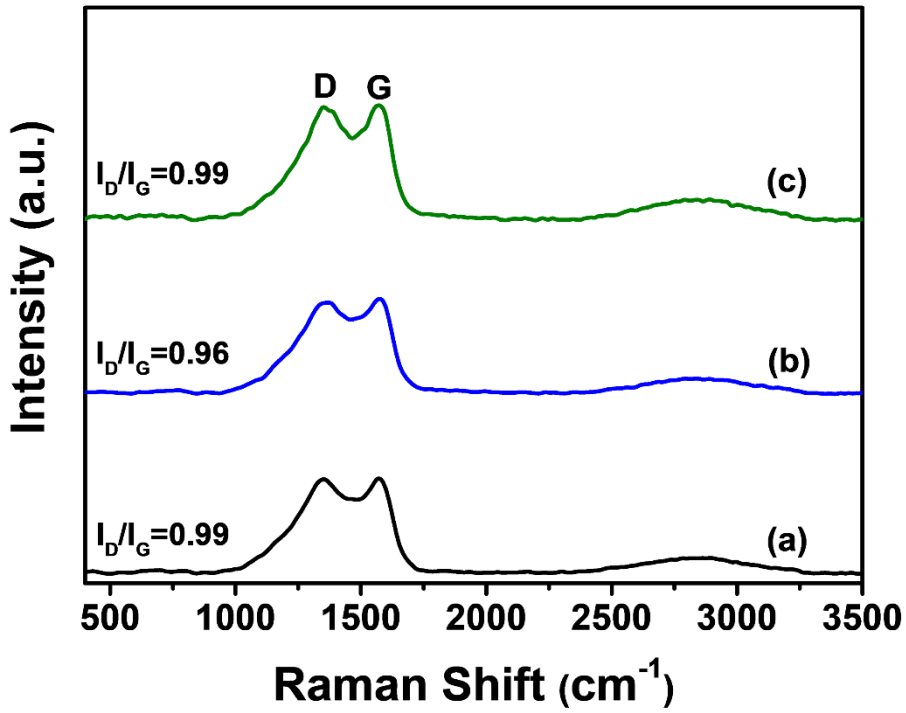

Figure S5. Raman spectra of NiUiO-bpydc-600 (a), Ni_1Fe_1UiO-bpydc-600 (b) and FeUiO-bpydc-600 (c) by the pyrolysis of the corresponding samples under 600 ºC.

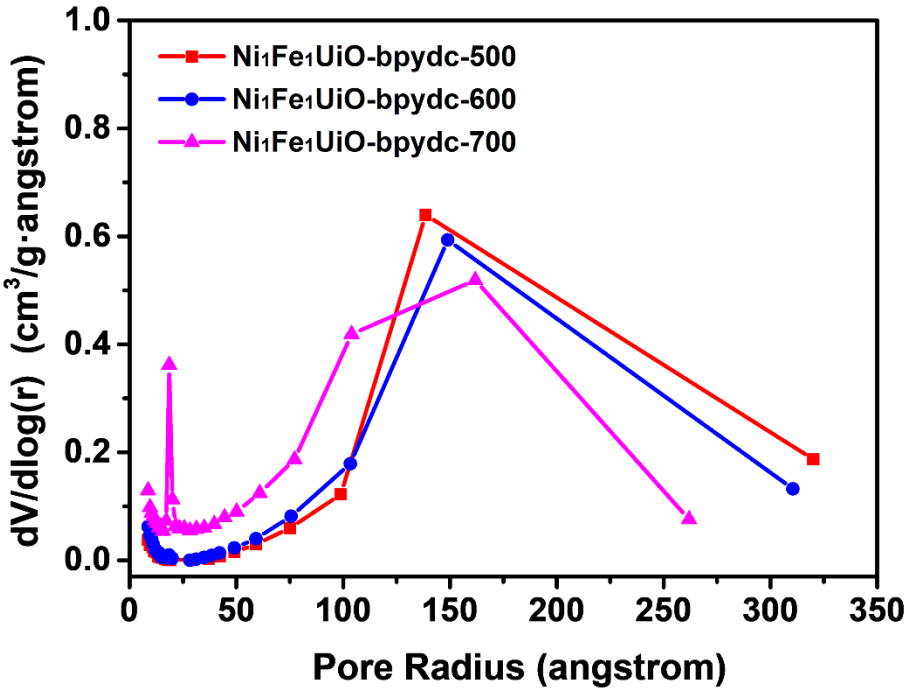

Figure S6. BJH Desorption Pore Distribution of Ni_1Fe_1UiO-bpydc-500, Ni_1Fe_1UiO-bpydc-600 and Ni_1Fe_1UiO-bpydc-700.

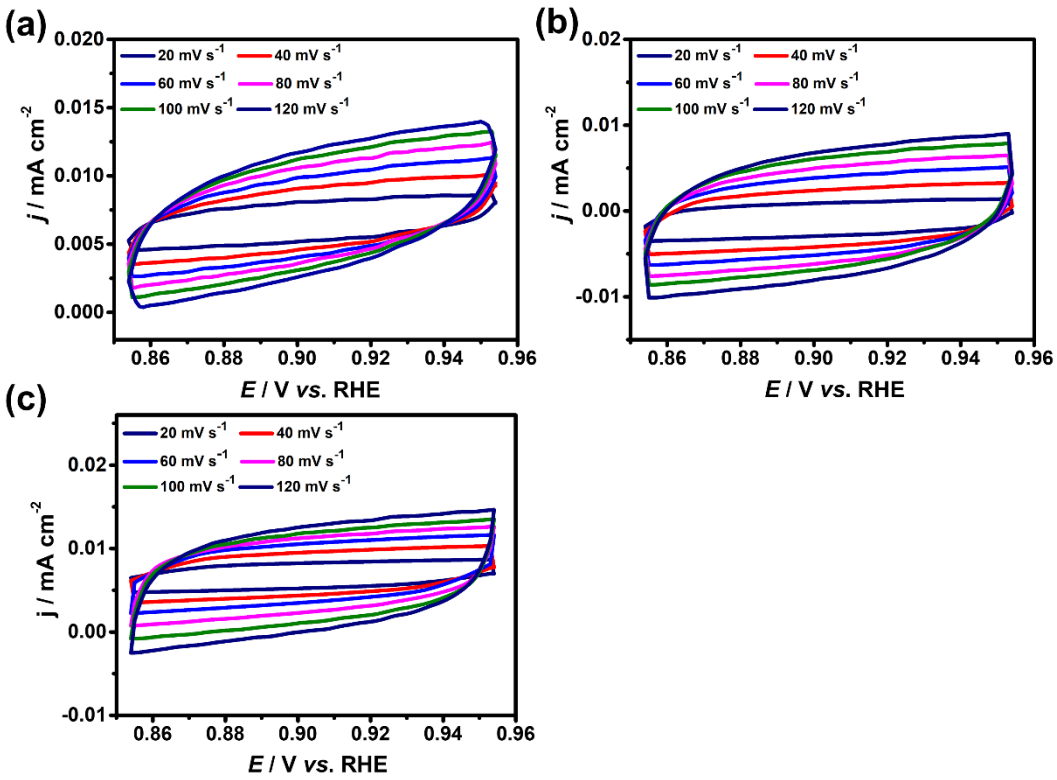

Figure S7. CVs curves of Ni_1Fe_1UiO-bpydc-500(a), Ni_1Fe_1UiO-bpydc-600(b) and Ni_1Fe_1UiO-bpydc-700(c) from 0.854 to 0.954 V (*vs.* RHE) at scan rates of 20,40,60,80,100,120 mV s^{-1} in 1.0 M KOH.

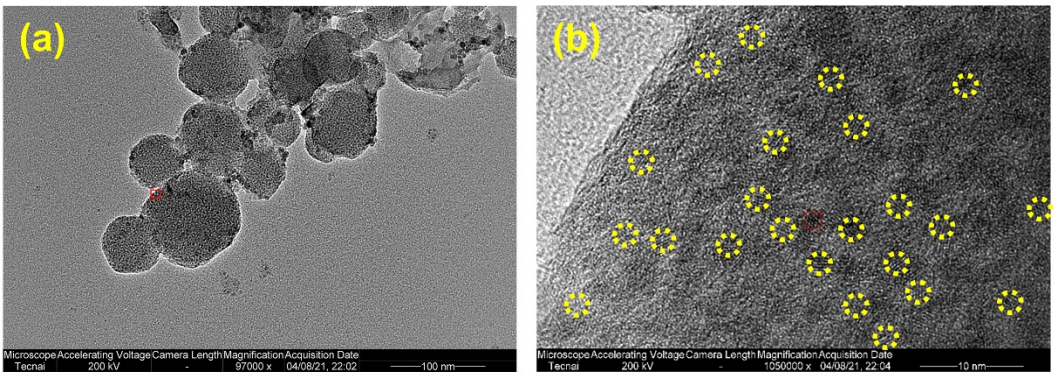

Figure S8. HRTEM images of the spent Ni_1Fe_1UiO-bpydc-600 by the long-term durability test performed by chronoamperometry after 43 h.

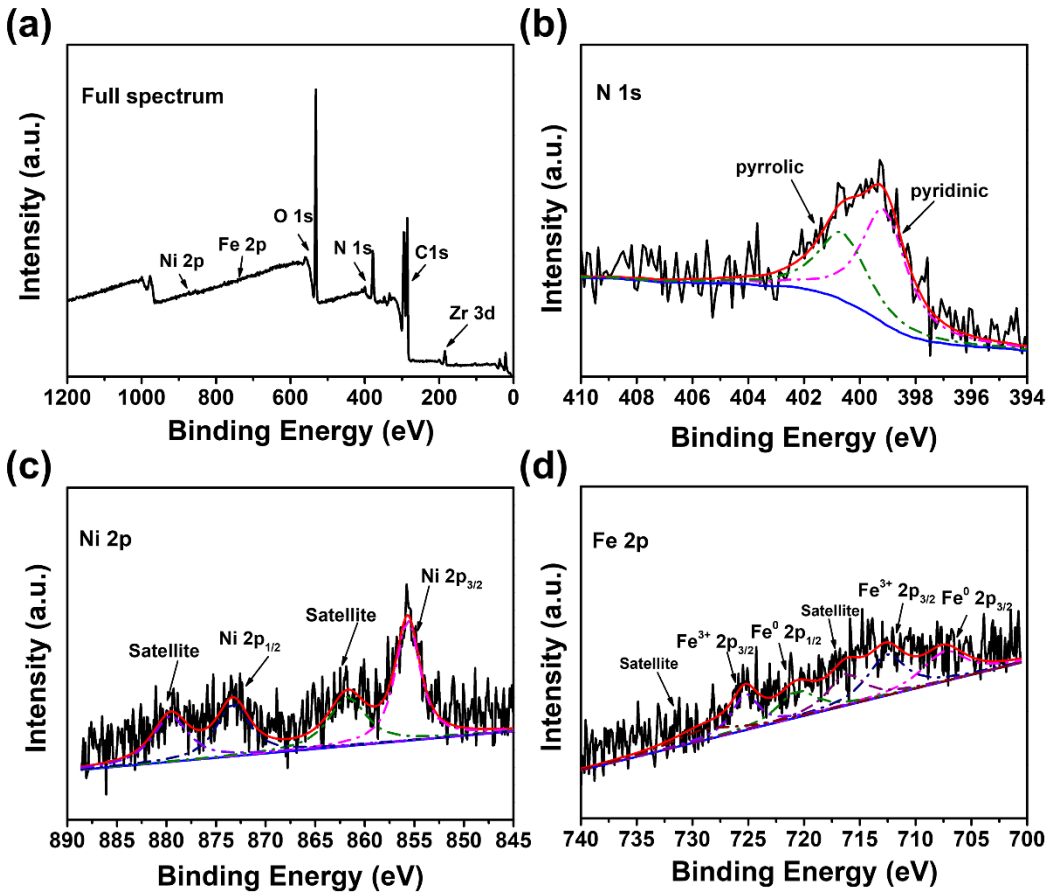

Figure S9. XPS spectra of the spent Ni_1Fe_1UiO-bpydc-600 by the long-term durability test performed by chronoamperometry after 43 h. (a) Full spectra; (b) High-resolution N 1s XPS spectra; (c) High-resolution Ni 2p XPS spectra; (d) High-resolution Fe 2p XPS spectra.

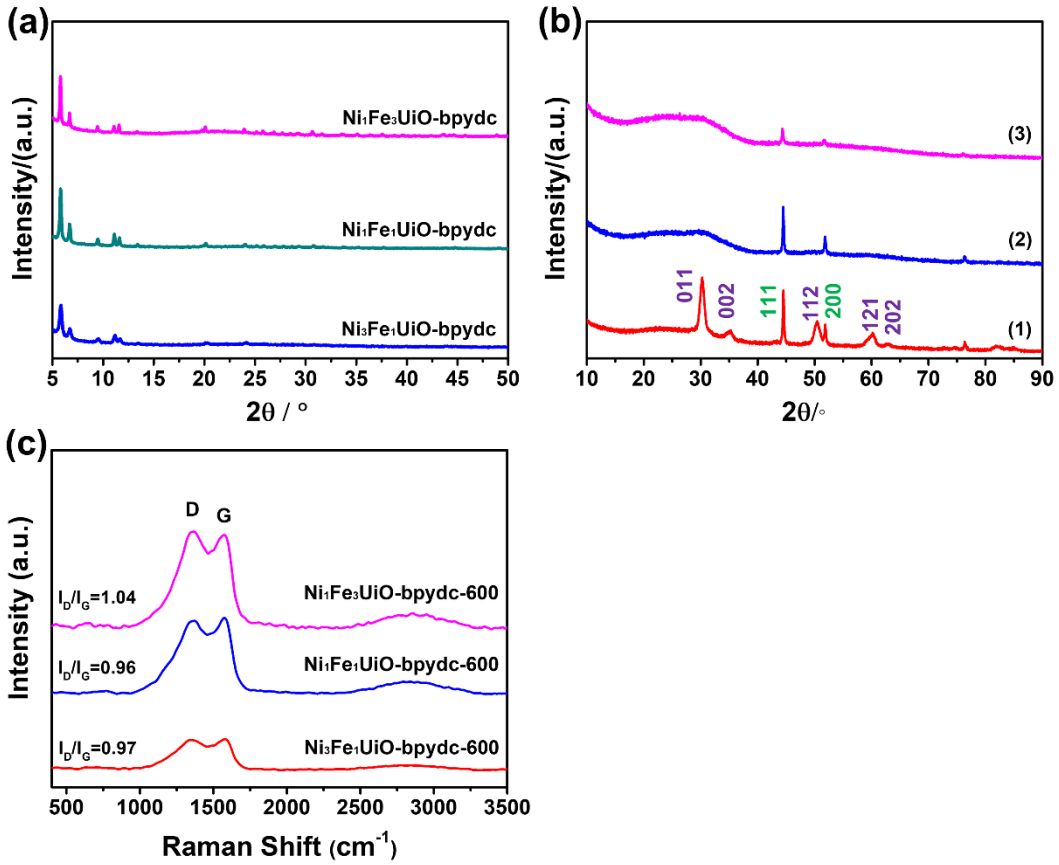

Figure S10. (a) PXRD patterns of the as-made relevant samples; (b) PXRD patterns of Ni_3Fe_1UiO-bpydc-600 (1), Ni_1Fe_1UiO-bpydc-600 (2) and Ni_1Fe_3UiO-bpydc-600 (3). (Green: PDF# 87-0712, Metallic Ni; Purple: PDF#50-1089, ZrO_2); (c) Raman spectra of the corresponding samples.

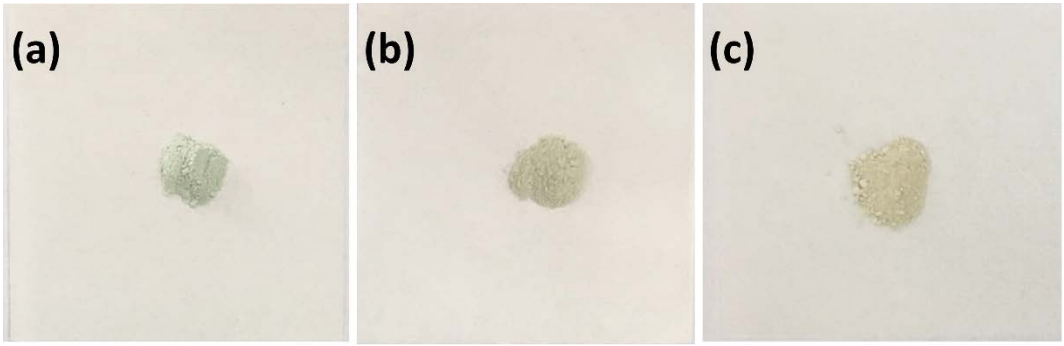

Figure S11. The optical photographs of Ni_3Fe_1UiO-bpydc (a), Ni_1Fe_1UiO-bpydc(b), Ni_1Fe_3UiO-bpydc(c)

Table S1. The fitting parameters in the equivalent circuit for different samples

Sample	R_{ct} /Ω	R_s /Ω	C_{dl} /μF	Chi-sqr
Ni_1Fe_1UiO-bpydc-500	46.8	731	15.9	0.006
Ni_1Fe_1UiO-bpydc-600	33.4	636	15.1	0.005
Ni_1Fe_1UiO-bpydc-700	46.6	1615	17.3	0.011
IrO_2	32.6	514	15.0	0.004

Table S2. OER performance comparison between Ni_1Fe_1UiO-bpydc-600 and those of MOF-derived Fe/Ni-based materials reported previously.

Catalysts	Overpotential@current density (mV@mA cm^{-2})	Tefel slope (mV dec^{-1})	Reference
Ni_1Fe_1UiO-bpydc-600	**372@10**	**84.4**	**This work**
FeNi@N-CNT	300@10	47.7	[S1]
Ni@NC-900	330@10	52	[S2]
FeCoNi	325@10	60	[S3]
NiCo2O4	380@10	50	[S4]
Ni MOF	346@10	64	[S5]
NGO/Ni_7S_6	380@10	45	[S6]
FeNi@N-CNT	300@10	47.7	[S7]
Co2Ni@NC	402@10	116	[S8]
Ni @ NiO/N-C nanowires	390@10	100	[S9]
0.50Ni/Co/NC	/	103	[S10]
Ni/Zn/Co/NC	/	112	[S11]
Fe-Co-CN/rGO-700	308@10	54	[S12]

References

[S1] Tao, Z. X.; Wang, T.; Wang, X. J.; Zheng, J.; Li, X. G. MOF-derived noble metal-free catalysts for electrochemical water splitting. ACS Appl. Mater. Interfaces 2016, 8, 35390-35397.

[S2] You Xu, Wenguang Tu, Bowei Zhang, Shengming Yin, Yizhong Huang, Markus Kraft, Rong Xu. Nanoparticles Encapsulated in Few-Layer NitrogenDoped Graphene Derived from Metal-Organic Frameworks as Efficient Bifunctional Electrocatalysts for Overall Water Splitting. Adv. Mater. 2017, 29, 1605957.

[S3] Yang Yang, Zhiyu Lin, Shiqi Gao, Jianwei Su, Zhengyan Lun, Guoliang Xia, Jitang Chen, Ruirui Zhang, Qianwang Chen. Tuning Electronic Structures of Nonprecious Ternary Alloys Encapsulated in Graphene Layers for Optimizing Overall Water Splitting Activity. ACS Catal. 2017, 7, 469-479.

[S4] Lei Han, Xin-Yao Yu, Xiong Wen (David) Lou. Formation of Prussian-Blue-Analog Nanocages via a Direct Etching Method and their Conversion into Ni-Co-Mixed Oxide for Enhanced Oxygen Evolution. Adv. Mater. 2016, 28, 4601-4605.

[S5] Viruthasalam Maruthapandian, Shanmugasundaram Kumaraguru, Dr. Subramanian Mohan, Dr. Velu Saraswathy, Dr. Srinivasan Muralidharan. An Insight on the Electrocatalytic Mechanistic Study of Pristine Ni MOF (BTC) in Alkaline Medium for Enhanced OER and UOR. ChemElectroChem, 2018, 5, 2795-2807.

[S6] Kolleboyina Jayaramulu, Justus Masa, Ondrej Tomanec, Daniel Peeters, Vaclav Ranc, Andreas Schneemann, Radek Zboril, Wolfgang Schuhmann, Roland A. Fischer. Nanoporous Nitrogen-Doped Graphene Oxide/Nickel Sulfide Composite Sheets Derived from a Metal-Organic Framework as an Efficient Electrocatalyst for Hydrogen and Oxygen Evolution. Adv. Funct. Mater. 2017, 27, 1700451.

[S7] Zixu Tao, Teng Wang, Xiaojuan Wang, Jie Zheng, Xingguo Li. MOF-Derived Noble Metal Free Catalysts for Electrochemical Water Splitting. ACS Appl. Mater. Interfaces 2016, 8, 35390-35397.

[S8] Xiaobin Liu, Xudong Zhao, Li-Zhen Fan. Boosting oxygen evolution reaction activity by tailoring MOF-derived hierarchical Co-Ni alloy nanoparticles encapsulated in nitrogen-doped carbon frameworks. RSC Adv., 2021, 11, 10874.

[S9] Aijuan Xie, Jie Zhang, Xiang Tao, Jianghui Zhang, Bingyan Wei, Wenhao Peng,Yuwei Tao, Shiping Luo. Nickel-based MOF derived Ni @ NiO/N-C nanowires with core-shell structure for oxygen evolution reaction. Electrochimica Acta 324 (2019) 134814.

[S10] Jiapeng Hua, Juan Chen, Hao Lina, Ruilai Liu, Xiaobing Yang. MOF derived Ni/Co/NC catalysts with enhanced properties for oxygen evolution reaction. Journal of Solid State Chemistry 259 (2018) 1-4.

[S11] Shengyun Zhao, Juan Chen. Metal organic framework-derived Ni/Zn/Co/NC composites as efficient catalyst for oxygen evolution reaction. Journal of Porous Materials (2019) 26:381-387.

[S12] Wenhui Fang, Jing Wang, Ye Hu, Xiaoqing Cui, Ruifeng Zhu, Yuhua Zhang, Chaochao Yue, Jiaqi Dang, Wei Cui, Hong Zhao, Zengxi Li. Metal-organic framework derived Fe-Co-CN/reduced graphene oxide for efficient HER and OER. Electrochimica Acta 365 (2021) 137384.